Calculations of second-harmonic generation for a jellium metal surface

W. L. Schaich
Physics Department, Indiana University, Bloomington, Indiana 47405
(Received 13 September 1999)

The microscopic a parameter, which alone is needed to describe the surface sensitive dependence of second-harmonic generation from jellium metals, is calculated within a time-dependent local-density-functional approximation for frequencies between zero and twice the bulk plasmon. The calculations incorporate an extrinsic damping and allow for the excitation of bulk plasmons. The results for frequencies up to half the bulk plasmon are very similar to earlier evaluations, while at higher frequencies only weak spectral structure is found.

I. INTRODUCTION

It has been more than ten years since microscopic calculations of second-harmonic generation (SHG) at simple metal surfaces were presented.[1,2] Several refinements have been made since then, including treatments of overlayers and estimates of crystalline effects; see the monograph by Liebsch for references and a review of this work.[3] However, in all the microscopic calculations on continuum models, one has kept the applied frequency below half the bulk plasmon frequency ω_p, where $\omega_p^2 = 4\pi n_b e^2/m$ with n_b the bulk density. This limitation was imposed in order to avoid the numerical problems caused by plasma waves generated at the surface and propagating into the bulk.

In this paper we show how these difficulties can be overcome, allowing calculations of SHG at all frequencies. The basic scheme is the same as in earlier work,[1–4] so we focus on the self-consistent, but nonretarded, dynamic second-order density response to an imposed electric field oscillating at frequency ω and directed normal to the surface. The dipole moment of this density response determines the a parameter, which in turn is the only surface sensitive quantity needed in a jellium model of a flat, clean surface to evaluate SHG for arbitrary polarizations and angles of incidence. Our results show surprisingly little structure in $a(\omega)$ for $\omega > \omega_p/2$. Even near the multipole mode ($\omega/\omega_p \simeq 0.8$) a has only a modest bump and then quickly settles back to its high-frequency limit of $a = -2$.

In Sec. II we discuss the changes in the numerical analysis that have allowed us to extend the calculations. The running time of the code is only slightly increased for $\omega > \omega_p/2$. Then in Sec. III we present results from a series of calculations over the range $0 < \omega < 2\omega_p$ for jellium models whose densities extend from $r_s = 2$ to $r_s = 5$.

II. THEORY

Consider first when bulk plasmons can arise in an SHG calculation. The bulk plasmon in jellium is a well-defined excitation only over a limited range of frequencies, starting at ω_p and cut off by the onset of Landau damping at ω_c. The ratio ω_c/ω_p depends on the bulk density and on the particular approximation used for exchange and correlation,[5,6] but typically lies between 1.3 and 1.5. This general feature leads to the calculation of SHG in different ways for separate frequency ranges.

For $\omega < \omega_p/2$ one can ignore bulk plasmons in both the linear and quadratic response, as has been done so far.[1–3] This freedom is also possible for $\omega > \omega_c$ and for $\omega_c/2 < \omega < \omega_p$. The latter range overlaps the multipole mode in the linear response; i.e., one can examine the SHG response for $\omega/\omega_p \approx 0.8$ with no change in computer code. For $\omega_p/2 < \omega < \omega_c/2$, the bulk plasmons enter the screening of the quadratic driving terms, but not into the linear response. On the other hand, for $\omega_p < \omega < \omega_c$, the bulk plasmons appear in the linear response, but may be ignored in the screening of the nonlinear terms. One never needs to account simultaneously for bulk plasmons in first- and second-order responses.

Our allowance for the bulk plasmon is a straightforward extension of the calculational scheme outlined recently.[7] We determine the induced densities $\rho_j(x, j\omega)$ at first and second order ($j = 1$ and 2) near the left side of a metal slab, which lies between capacitor plates that apply the spatially constant normal field E_A at frequency ω. The spatial range kept in the numerical evaluation runs along the normal coordinate from x_v in vacuum to $x_c = L$ well inside the metal. When a bulk plasmon may be present we assume that the relevant induced charge density is not negligible near $x = L$, but instead varies as

$$\rho_j(x, j\omega) \approx \rho_j(L, j\omega) e^{ip_j(x-L)} \tag{1}$$

for $x \geq L$.

The complex-valued wave vector $p_j = p(j\omega)$ of the plasmon is a bulk property determined by fitting the imaginary part of the inverse bulk dielectric function $(1/\epsilon_b)$ to a Lorentzian shape. Our motivation here comes from the fact that in a hydrodynamic model $1/\epsilon_b$ has the form[8]

$$\frac{1}{\epsilon_b^{\mathrm{H}}} - 1 = \frac{\omega_p^2/\beta^2}{p^2 - q^2}, \tag{2}$$

as a function of the three-dimensional (3D) momentum q for a fixed frequency ω. Here $\beta^2 = \frac{3}{5} v_F^2$ with v_F the Fermi velocity. From the location and width of the peak in $-\mathrm{Im}(1/\epsilon_b)$ versus q^2 for a general dielectric function we can determine an effective value of p^2. The dielectric functions we use in this recipe have the form

$$\frac{1}{\epsilon_b} - 1 = \frac{\chi_b v}{[1 - \chi_b(v + V_{xc})]}, \tag{3}$$

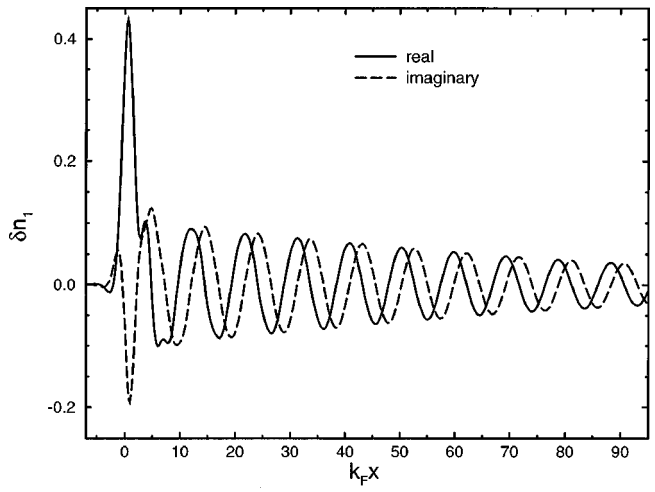

FIG. 1. First-order-induced charge density versus normal coordinate at $\omega/\omega_p=1.2$. A bulk plasmon with wave vector $p/k_F=0.66+i0.014$ is responsible for the long-ranged, oscillatory tail.

where χ_b is the bulk Lindhard susceptibility,[5,9] $v=4\pi e^2/q^2$, and $V_{xc}=\partial^2/\partial n^2(n\epsilon_{xc})$ evaluated at $n=n_b$. Here ϵ_{xc} is the average exchange-correlation energy per electron in a bulk system of density n. Equation (3) derives from a local-density-functional approximation (LDA), and if one ignores V_{xc} it becomes the random-phase approximation (RPA).

Given the ansatz (1) for the induced density beyond $x=L$, we find an additional potential energy

$$e\Delta\varphi_j(x,j\omega)=e\rho_j(L,j\omega)\times\begin{cases}\left[\dfrac{4\pi}{p_j^2}+V_{xc}/e^2\right]e^{ip_j(x-L)}, & L<x,\\ \dfrac{4\pi}{p_j^2}[1+ip_j(x-L)], & x<L.\end{cases}\tag{4}$$

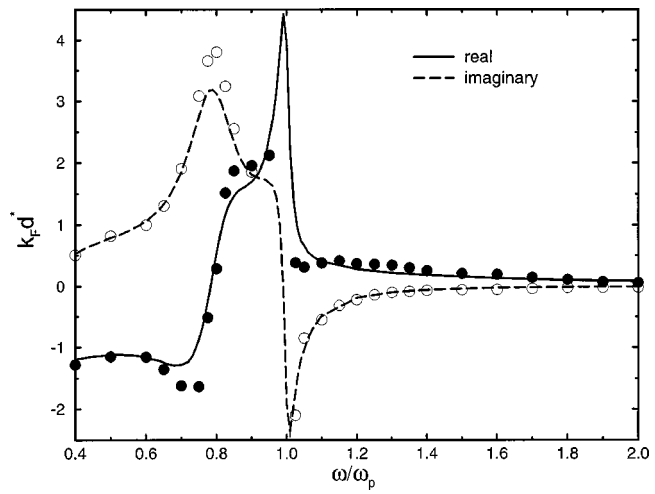

FIG. 2. Complex conjugate of the d parameter versus frequency. The smooth curves are from the present calculation while the circles are from data in Ref. 6, which used a different approximation for ϵ_{xc} and no damping. A bulk plasmon is present for $1.0<\omega/\omega_p<1.36$.

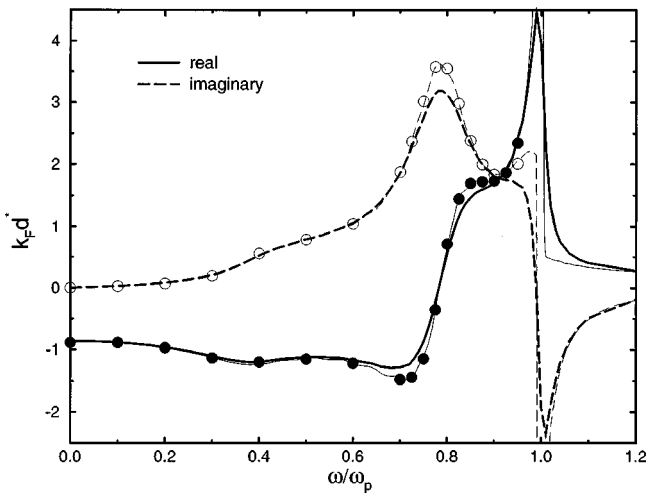

FIG. 3. Complex conjugate of the d parameter versus frequency. The smooth curves are from the present calculation; the thick lines have $\gamma/\omega_F=0.02$, while the thin lines have $\gamma/\omega_F=0.0001$. Aside from the different γ values, nothing else was changed. The circles are from data in Ref. 15, which used the same approximation for ϵ_{xc} and no extrinsic damping. They are constrained to have $\omega<\omega_p$.

The contributions to $\Delta\varphi_j$ include both the Hartree term and an LDA estimate of exchange and correlation energies. The simple form of $\Delta\varphi$ in $x>L$ allows us to analytically do integrals for $x\to\infty$ of products of $\Delta\varphi$ and a nonlocal susceptibility. There is also no problem with the numerical evaluation of such integrals for $x_v<x<L$. Hence the additional induced charge density due to $\Delta\varphi$ may be readily determined and incorporated into the mean-field equations that determine the total induced charge density.[7]

As mentioned above, our basic numerical scheme is described in Ref. 7. Rather than reproduce the various derivations done there, we only note several ways in which our procedures differ from those of Liebsch.[3] We do not introduce model densities when solving the response equations, but we do allow the frequency to have a significant imaginary part: $\omega\to\tilde{\omega}=\omega+i\gamma$, where $\hbar\gamma$ is a few percent of the Fermi energy. The presence of γ reduces numerical problems because it causes all induced quantities to decay as x moves into the bulk. However, γ also smoothes out the frequency dependence of the response, so one should not make γ too large. There can be experimental estimates of γ since 2γ corresponds to the Drude scattering rate.[7] Consideration of all of these constraints leads to the γ values we have chosen, but we also show how results vary with γ.

For SHG one needs the a parameter formally defined by[7]

$$a=8\rho_b\int dx\, x\rho_2(x,2\omega)/\sigma_1^2,\tag{5}$$

TABLE I. Parameter choices.

r_s	$V/\hbar\omega_p$	$-k_Fx_v$	k_FL	$k_F\Delta x$	γ/ω_F
2	0.981	12.8	94.2	0.2	0.02
3	0.997	10.0	92.4	0.2	0.02
4	1.053	12.0	77.55	0.15	0.03
5	1.118	10.5	77.1	0.15	0.04

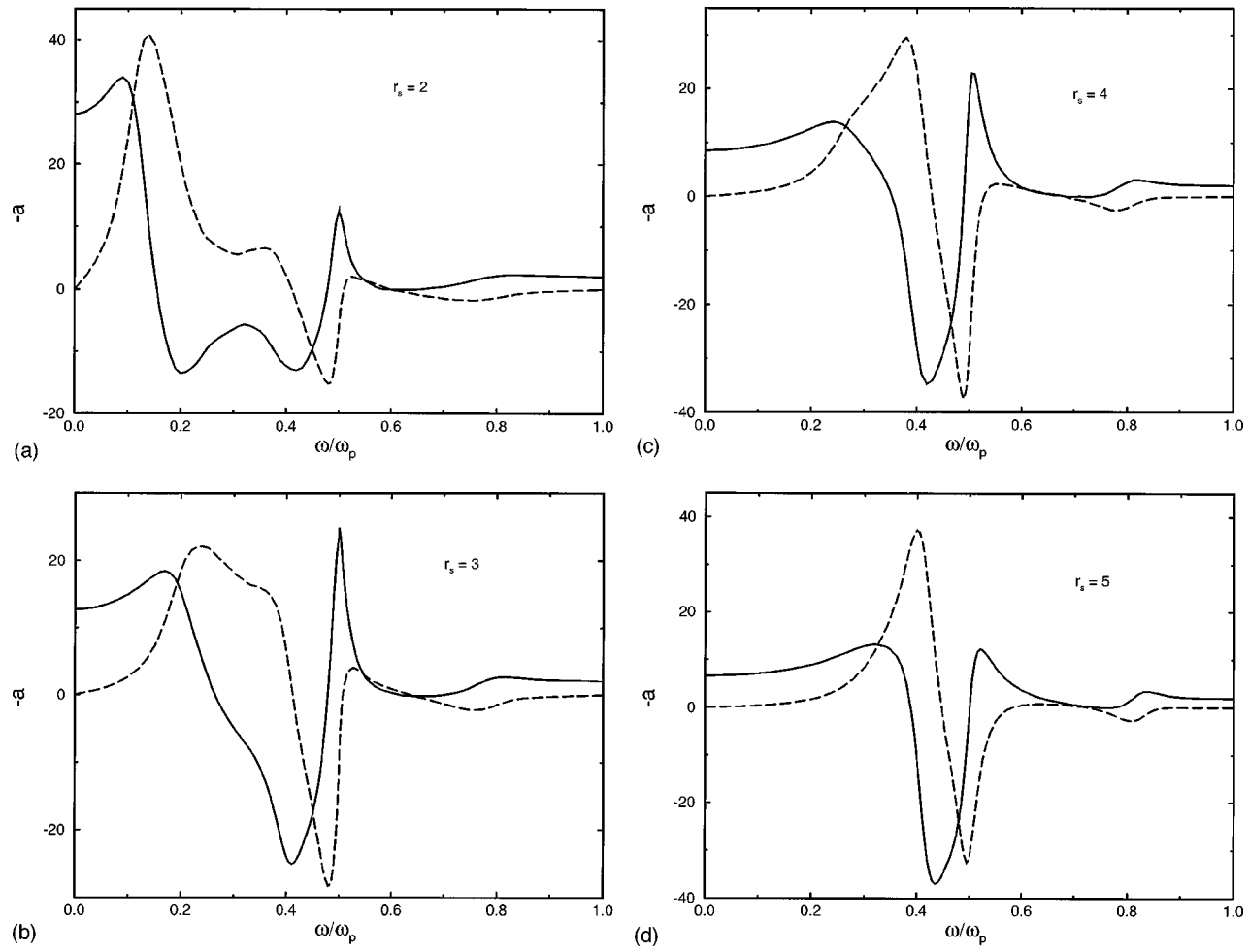

FIG. 4. Plots of the a parameter versus frequency. The parameters of the calculations are in Table I and in all panels the solid (dashed) curves are the real (imaginary) parts of $-a$.

with $\rho_b = e n_b$, but actually evaluated from

$$a = -2 + 8\left(1 - \frac{4\tilde{\omega}^2}{\omega_p^2}\right)^{-1}\left\{\int_{x_v}^{0} dx\, x\rho_2(x,2\omega) + \int_{x_v}^{L} dx\, \rho_2(x,2\omega) F_{\rm ext}(x)/m\omega_p^2\right\}\rho_b/\sigma_1^2. \qquad (6)$$

Here $x=0$ is the jellium edge, $\sigma_1 = \int dx\, \rho_1(x,\omega)$, and in an LDA calculation $F_{\rm ext}$ vanishes. For an RPA calculation $F_{\rm ext} = -\partial\mu_{xc}^{(0)}/\partial x$ with $\mu_{xc}^{(0)} = \partial/\partial n(n\epsilon_{xc})$ evaluated at $n = n_0(x)$, where $n_0(x)$ is the ground-state electron energy profile for the slab. The sum rule that allows one to jump from Eq. (5) to Eq. (6) corrects the (small) error in Ref. 2 and agrees with Ref. 3. It is important that one can avoid trying to calculate the integral of $x\rho_2$ over all x.

At several places in the calculation one does analytically integrals that are slowly convergent. One example is the driving term in second order due to the potential energy associated with the bulk electric field, $E_{\rm A}/(1-\omega_p^2/\tilde{\omega}^2)$. The potential energy associated with the outside electric field also grows linearly in magnitude with distance from the surface, but usually this causes no problem because the susceptibility it multiplies is decaying exponentially as one moves that coordinate out into vacuum. However, in one part of the second-order response there can be difficulties when $\hbar\omega$ exceeds the work function. In that case part of the susceptibility [A_2 in Eq. (23) of Ref. 7] can be nondecaying in a coordinate (x_a) that is to be multiplied by the first-order potential energy and integrated to $-\infty$ in vacuum. Liebsch suppresses this difficulty by cutting off the integral at x_v.[10] We go one step farther to integrate analytically with the Hartree part of the potential energy, which is a linear function of x. However, like Liebsch, we truncate the integral with the exchange-correlation contributions at x_v. This term is not present in RPA and the difficulties it implies in LDA seem unphysical. The total potential energy in first order, outside the metal, is to within a constant

$$e\varphi_1(x<x_v,\omega) = -exE_{\rm A} + \mu_{xc}'(x)\rho_1(x,\omega)/e, \qquad (7)$$

where $\mu_{xc}' = \partial^2/\partial n^2(n\epsilon_{xc})$ evaluated at $n = n_0(x)$. As a rough estimate $\epsilon_{xc} \sim n^{1/3}$, so $\mu_{xc}' \sim n_0^{-2/3}$, while $\rho_1 \sim n_0^{1/2}$. Thus the exchange-correlation contribution to $e\varphi_1$ outside eventually diverges as $n_0^{-1/6}$ as x moves far away. However, this formal divergence does not become apparent until x is tens of Angstroms outside[11] and in a domain where an LDA is not reliable. Hence the *ad hoc* truncation of this part of φ_1 is not unreasonable. We did check that moving x_v around by a few Angstroms does not significantly change our results.

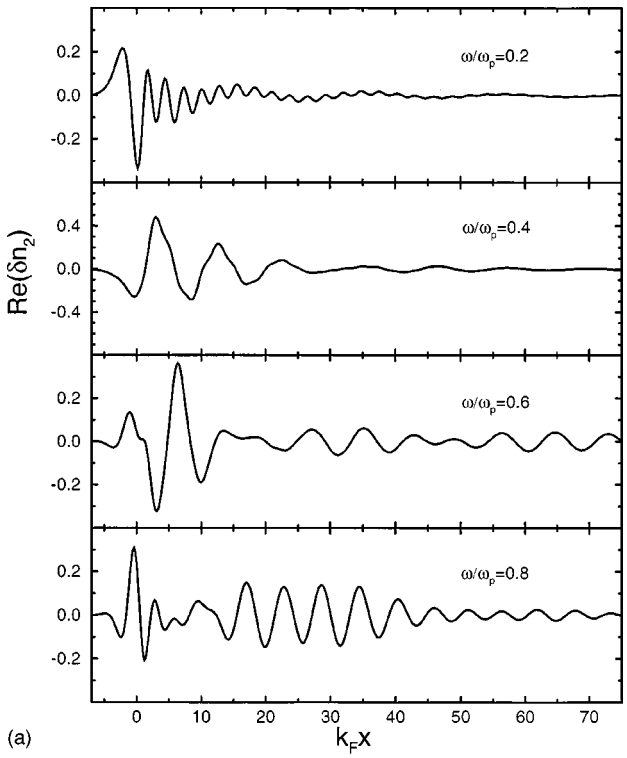

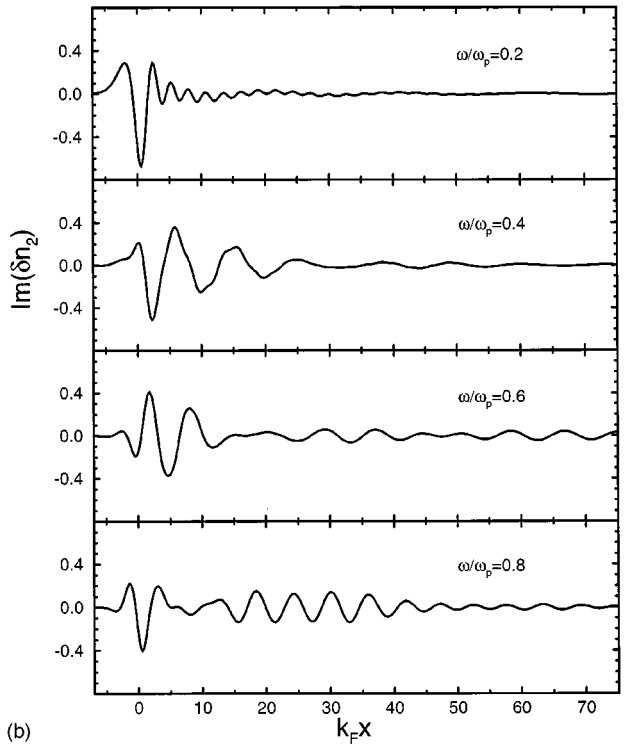

FIG. 5. Second-order-induced charge density versus normal coordinate for several frequencies. The scale for the ordinate changes between the panels. See Table I for the parameters used in these $r_s=3$ calculations.

III. RESULTS

We begin with some linear response properties. Figure 1 shows the first-order LDA charge density when $\omega/\omega_p=1.2$. The bulk density has $r_s=3$ and $\gamma/\omega_F=0.02$, where ω_F is the Fermi frequency. The dimensionless ordinate is $\delta n_1(x,\omega)$ $=\rho_1(x,\omega)/k_F\sigma_1$, with k_F the Fermi wave vector, and is normalized so its integral over k_Fx equals one. The bulk cutoff is at $k_FL=62.4$ and Eq. (1) is used to plot beyond $x=L$. This ansatz looks very reasonable here.

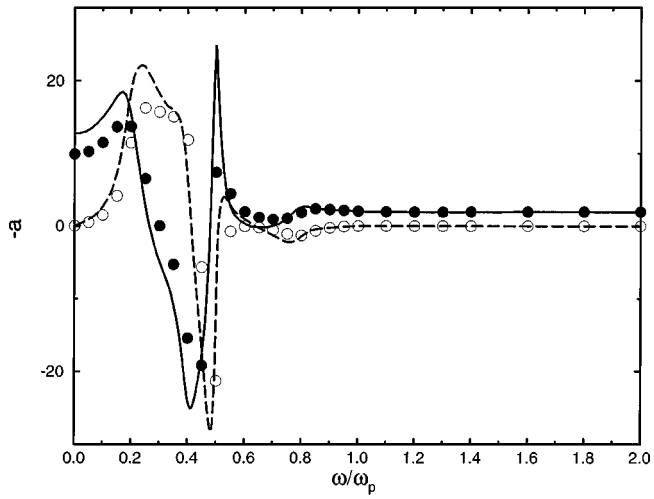

FIG. 6. Comparison of plots of a parameter versus frequency. The curves (circles) are from an LDA (RPA) calculation. The LDA results extend the plot in Fig. 4.

In Fig. 2 we plot the d parameter defined by

$$d=\int dx\, x\rho_1(x,\omega)/\sigma_1 \tag{8}$$

but actually evaluated from

$$d=(1-\tilde{\omega}^2/\omega_p^2)^{-1}\left\{\int_{x_v}^{0} dx\, x\rho_1(x,\omega) + \int_{x_v}^{L} dx\, \rho_1(x,\omega)F_{\rm ext}(x)/m\omega_p^2\right\}/\sigma_1. \tag{9}$$

The equivalence of these two expressions is based on another sum rule,[12,3] and for the LDA results shown $F_{\rm ext}\equiv 0$. We are

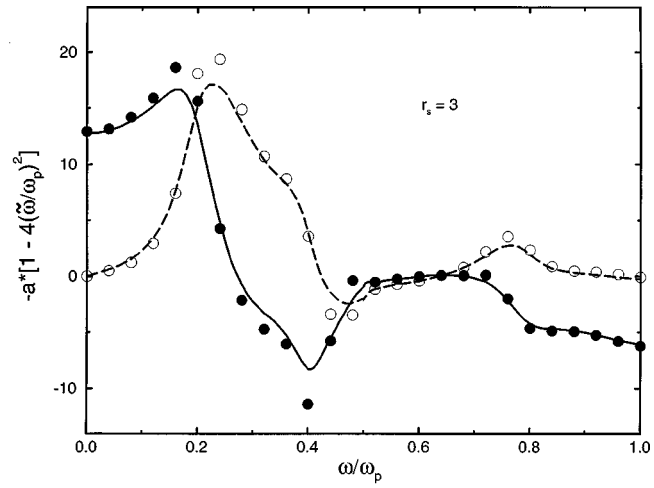

FIG. 7. Dependence of the a parameter on the choice of damping. The curves (circles) use $\gamma/\omega_F=0.02(0.001)$ with no other changes from the $r_s=3$ line of Table I. The factor multiplying a suppresses sharp structure near $0.5\omega_p$.

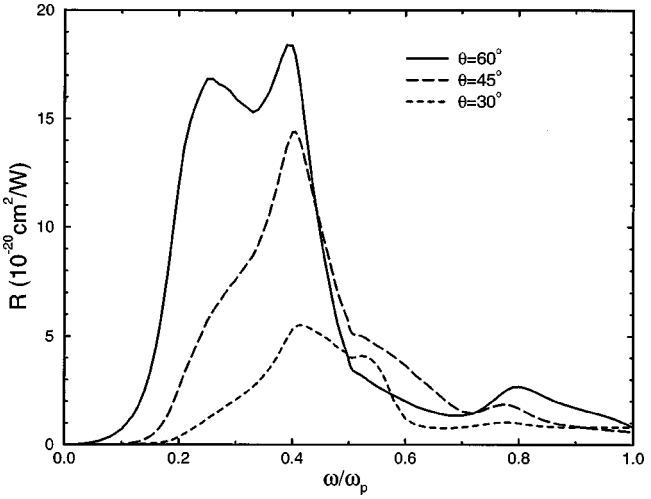

FIG. 8. Second-harmonic radiation efficiency for different angles of incidence. The only microscopic quantity used is the a for $r_s=3$ of Fig. 4.

using the Wigner interpolation formula for the correlation part of ϵ_{xc} (Ref. 13) and again take $\gamma/\omega_F=0.02$ but push the cutoff out to $k_FL=92.4$. The curves compare reasonably with the data from Ref. 6 which used a momentum-space evaluation with $\gamma=0^+$ and a different approximation for the correlation energy.[14]

To show that most of the slight differences in Fig. 2 can be removed, we compare in Fig. 3 our same calculation with Liebsch's results,[12,15] which used the Wigner form of ϵ_{xc} and set $\gamma=0^+$. There are clear differences only near regions of sharp variation, and these essentially go away if we reduce our damping to $\gamma/\omega_F=0.001$. It is remarkable that for $\omega/\omega_p<0.6$ and $\omega/\omega_p>1.1$ that the d parameter is only weakly dependent on γ. This eventually ceases to be true for larger values of γ, such as the $\gamma/\omega_p=0.05$ used by Gies and Gerhardts.[6,15,16]

Turning now to the nonlinear response we show in Fig. 4 the a parameter versus frequency for jellium surfaces with different bulk densities. Parameter choices for the different cases are listed in Table I. The step size for the real-space mesh is Δx, and the ground-state barrier heights for the confining potential energy are V. It is remarkable that V is nearly $\hbar\omega_p$ for all r_s. We used a smaller step size (relative to the Fermi wavelength) at larger r_s since the barrier becomes a sharper structure on this scale as r_s increases.[3,13]

The spectral variation of a for $\omega<\omega_p/2$ has been amply discussed by Liebsch.[1–3] Even with the various differences in calculation noted in Sec. II, we still obtain the same qualitative behavior. At the higher bulk densities (smaller r_s), structures due to 2ω matching the work function or the multipole (near $0.8\ \omega_p$) are well separated. As r_s increases and the work function becomes a larger fraction of the total barrier height, the emission threshold structure shifts upward to merge into the multipole structure.

The completely new results are for $\omega>\omega_p/2$, which for all r_s show rather little structure. There is a small bump when the first harmonic frequency crosses the multipole resonance near $0.8\ \omega_p$. This structure is stronger for larger r_s, but it is never dominant as predicted by recent hydrodynamic model calculations.[17] These authors used equilibrium surface density profiles that were either linear or quadratic in shape with parameters chosen to fit the multipole location in linear response. Their predicted a's near $0.8\ \omega_p$ are several orders of magnitude larger than our results in Fig. 4. The older hydrodynamic calculations[4,18] which used a two-step surface density profile do predict a structure in a comparable to that shown in Fig. 4 near $0.8\ \omega_p$, but also predict further structures at higher frequency, which do not appear here. The high-frequency limit of a is -2,[19] which requires that the integrals with ρ_2 in Eq. (6) become negligible. It is surprising that this happens even before $\omega>\omega_p$.

To provide more insight we show in Fig. 5 plots of the second-order-induced density at various frequencies for a system with $r_s=3$ and corresponding parameters from Table I. The dimensionless variable $\delta n_2=\rho_b\rho_2(x,2\omega)/k_F^2\sigma_1^2$. Although to find a from Eq. (6) one needs in LDA the profile of $\rho_2(x,2\omega)$ only for $x<0$, the calculation of the whole profile must be self-consistent. As Fig. 5 illustrates, there is considerable evolution of these profiles as ω changes. The penetration of δn_2 into the bulk varies with frequency and a complicated pattern of Friedel oscillations appears. Although one can easily identify at low frequencies the dominant Friedel period,[2,3] we have not been able to do this over the midrange of frequencies.[20] At the lowest frequencies the dominant Friedel wave vector is near $2k_F$. As ω/ω_p increases through 0.2 to 0.4, δn_2 extends farther into the bulk and develops a new oscillation pattern with a smaller wave vector. The effective wave vector of these Friedel oscillations increases linearly with frequency,

$$q/k_F\approx 0.8(\omega/\omega_F), \tag{10}$$

an empirical relation that roughly holds for $2\leqslant r_s\leqslant 5$ but for which we have no *a priori* justification. There are several candidate wave vectors that might be important,[2,15,21] and these can be combined in various ways from the driving terms and screening processes of the nonlinear response. This perhaps explains why it is sometimes difficult to identify a single wave vector in the ''tail'' of δn_2.

For instance at $\omega/\omega_p=0.6$, there appear to be beats in the oscillation pattern. The bulk plasmon which can be excited in the screening of the nonlinear terms at 2ω has a wave vector $p/k_F\approx 0.66$, but its influence is not obvious. Our ansatz of Eq. (1) does not seem appropriate for this case. Fortunately the oscillations, although very long ranged, are fairly rapid. This implies that δn_2 for $x<0$ is not very sensitive to what is happening near the bulk cutoff. We found similar results for a upon changing L or even switching to a code that ignores any δn_2 (due to a bulk plasmon or whatever) beyond $x=L$.

Once ω exceeds ω_p the variation of δn_2 simplifies. The Friedel oscillations are then controlled by the plasmon wave vector, or beyond ω_c, by the wave vector at the edge of the particle-hole continuum into which the plasmon has merged.[6] Furthermore, δn_2 does not exceed 0.1 in either its real or imaginary part, which partially explains why $a\approx -2$. This limiting behavior holds for both LDA and RPA evaluations, as shown in Fig. 6. The differences between LDA and RPA results occur mostly below $\omega/\omega_p=0.5$ and are very similar to the earlier evaluations.[2] The qualitative

appearance of the spectrum of a does not depend on the treatment of exchange and correlation.

The structures we have found in a are generally much broader than the value of γ we have used. The only exception is near 0.5 ω_p, but this is misleading. In the equation for the intensity of second-harmonic radiation,[2–4] a is multiplied by the dielectric constant at 2ω, which nearly vanishes at 0.5 ω_p. Hence in Fig. 7, which illustrates how a depends on the damping parameter, we have multiplied a by $[1-(2\tilde{\omega}/\omega_p)^2]$ to suppress the rapid variation of a near 0.5 ω_p. The results are then qualitatively similar to those in Fig. 3. The plots depend noticeably on γ only near regions of sharp structure, at least for γ/ω_F smaller than a few percent. We remark that the various rescaling improvements discussed in Ref. 7 are important for producing stable numerical results when γ/ω_F is reduced to 0.001.

Finally, we close with Fig. 8 which shows the radiation efficiency predicted by our calculated a. Both the incident beam at ω and the exiting beam at 2ω are presumed to be p polarized. To evaluate the standard equations[2–4] as a function of the angle of incidence and driving frequency one only needs $a(\omega)$. Below 0.5 ω_p there are two strong structures, associated with the photoemission threshold and the multipole mode.[1–3] Above 0.5 ω_p there is only a single bump which arises from the excitation of the multipole mode by the first harmonic. The existence of this ''peak'' is no surprise but its relative strength is. The electron gas seems to quickly lose its nonlinearity as the frequency grows past 0.5 ω_p.

ACKNOWLEDGMENTS

We are grateful to Eric Goff and Ansgar Liebsch for helpful discussions. Part of the calculations were done on the Cray Research Inc. T90 system at NPACI in San Diego, CA.

[1] A. Liebsch, Phys. Rev. Lett. **61**, 1233 (1988); **61**, 1897(E) (1988).
[2] A. Liebsch and W.L. Schaich, Phys. Rev. B **40**, 5401 (1989).
[3] A. Liebsch, *Electronic Excitations at Metal Surfaces* (Plenum, New York, 1997).
[4] W.L. Schaich and A. Liebsch, Phys. Rev. B **37**, 6187 (1988).
[5] D. Pines and P. Nozières, *The Theory of Quantum Liquids* (Benjamin, New York, 1966).
[6] K. Kempa and W.L. Schaich, Phys. Rev. B **39**, 13 139 (1989).
[7] J.E. Goff and W.L. Schaich, Phys. Rev. B **61**, 10 471 (2000).
[8] W.L. Schaich, Phys. Rev. B **31**, 3409 (1985).
[9] R.R. Gerhardts and K. Kempa, Phys. Rev. B **30**, 5704 (1984).
[10] A. Liebsch (private communication).
[11] J.E. Goff (private communication).
[12] A. Liebsch, Phys. Rev. B **36**, 7378 (1987).
[13] N.D. Lang, in *Solid State Physics: Advances in Research and Applications*, edited by H. Ehrenreich, F. Seitz, and D. Turnbull (Academic, New York, 1973), Vol. 28, p. 225.
[14] L. Hedin and B.I. Lundqvist, J. Phys. C **4**, 2064 (1971).
[15] K. Kempa, A. Liebsch, and W.L. Schaich, Phys. Rev. B **38**, 12 645 (1988).
[16] P. Gies and R.R. Gerhardts, Phys. Rev. B **36**, 4422 (1987).
[17] J.A. Maytorena, W.L. Mochan, and B.S. Mendoza, Phys. Rev. B **51**, 2556 (1995).
[18] M. Corvi and W.L. Schaich, Phys. Rev. B **33**, 3688 (1986).
[19] B.S. Mendoza and W.L. Schaich, Bull. Am. Phys. Soc. **36**, 768 (1991).
[20] Note that Fig. 2 of Ref. 2 is flawed. It also does not consider a wide range of frequencies because of the calculational constraint $\omega/\omega_p < 0.5$.
[21] P.J. Feibelman, Phys. Rev. B **9**, 5077 (1974).